GEOPHYSICS, VOL. 61, NO. 3 (MAY-JUNE 1996); P. 646-665, 15 FIGS. AND 2 TABLES.

Quasi-linear approximation in 3-D electromagnetic modeling

Michael S. Zhdanov* and Sheng Fang*

ABSTRACT

The Born approximation in electromagnetic (EM) numerical modeling has limited application for solving 3-D electromagnetic induction problems, because in structures with high conductivity contrasts and at high frequencies, this approximation is inaccurate. In this paper, we develop a new and relatively simple approximation for the EM field called a *quasi-linear approximation,* which is based on the evaluation of the anomalous field E^a by a linear transformation of the normal (primary) field: $E^a = \hat{\lambda}\mathbf{E}^n$, where $\hat{\lambda}$ is called the *electrical reflectivity tensor.* The reflectivity tensor inside inhomogeneities can be approximated by a slowly varying function that can be determined numerically by a simple optimization technique. The new approximation gives an accurate estimate of the EM response for conductivity contrasts of more than one hundred to one, and for a wide range of frequencies. It also opens the possibility for fast 3-D electromagnetic inversion.

INTRODUCTION

One important approach to (EM) electromagnetic numerical modeling is based on linearization of the integral equations for scattered EM fields. This approach is usually called the *Born approximation* .

The Born approximation was developed originally to describe quantum mechanical scattering (Born, 1933). Since the basic idea behind this method has broad applications, it is possible to apply the Born approximation to different geophysical problems as well. For example, it has been used quite extensively and successfully in seismic geophysics (Bleistein and Gray, 1985), (Tarantola, 1987).

Let us formulate the general EM induction problem so that the unknown material parameter ("anomalous" parameter) can be treated as a perturbation from a known background (or "normal") parameter distribution. The solution of the induction problem in this case contains two parts: 1) a linear part, which can be interpreted as a direct scattering of the source field by the inhomogeneity without taking into account coupling between scattering currents, and 2) a nonlinear part that is composed of the combined effects of the unknown perturbation and the unknown scattered field at the inhomogeneous structure. The Born approximation is based on the assumption that this last part, which represents the actual nonlinearity of the physical problem, is negligible as compared to the linear part. As a result, a linear expression is obtained for the solution of the EM induction problem. This makes the method especially attractive for geophysical applications.

The perturbation methods have found numerous applications in 2-D electromagnetic modeling problems (Berdichevsky and Zhdanov, 1984). The Born approximation has been used widely in inversion schemes because it provides a linearized approach to the solution of inversion problems (Oristaglio, 1989; Habashy et al., 1986). However, the Born approximation works reasonably well only for small conductivity contrasts, relatively small inhomogeneities, and low frequencies ω (Born and Wolf, 1980; Habashy et al., 1993). It has limited application for solving general 3-D electromagnetic induction problems because the Born approximation breaks down when the anomalous induction number of the anomalous region, that is $\omega \mid \mu \mid \Delta\sigma \mid L^2$ (where L is the upper bound of the distance of any two points belonging to the region D with anomalous conductivity $\Delta\sigma$, and μ is the magnetic permeability) gets too large. It also has problems for high contrast bodies even at dc.

A novel approximation to numerically simulate the electromagnetic response of dipole or line sources in the presence of inhomogeneous structure has been introduced in Habashy et al. (1993) and applied to the inversion in Torres-Verdin and Habashy (1994). The authors of these papers present a new approximation for the scattered field inside inhomogeneous structure. This new approximation for the internal field is given by the projection of the background or normal electric field (i.e., the electric field excited in the absence of conductivity inhomogeneity) onto a scattering tensor. It is shown that the scattering tensor does not depend on the illuminating sources

Manuscript received by the Editor December 12, 1994; revised manuscript received August 2, 1995.
*University of Utah, Dept. of Geology and Geophysics, Salt Lake City, UT 84112.

and is a nonlinear functional of the anomalous conductivity distribution. In addition, papers (Habashy et al., 1993; Torres-Verdin and Habashy, 1994) demonstrate the efficiency of the new approximation, which remains accurate within a wide-frequency band for large anomalous structures and large conductivity contrasts.

Here, we present a different approach to the solution of the EM induction problem, which is based, however, on similar ideas and can be considered as a development of the Torres-Verdin and Habashy method. We separate the total electric field into normal and anomalous parts and introduce an electrical reflectivity tensor that linearly transforms the normal field into an internal anomalous one.

The electrical reflectivity tensor inside inhomogeneities can be approximated by slowly varying functions and can be determined numerically by a simple optimization technique. Thus we avoid a complicated problem of determining the scattering tensor and at the same time reach the desired result-to obtain a very precise approximation for the scattered field. We call this new and relatively simple approximation for the EM field a *quasi-linear (QL) approximation* because it generates an integral expression for the scattered field that is nonlinear with respect to the conductivity, but which is linear with respect to the product of the conductivity and the reflectivity tensor. It can be applied with the same efficiency to 2-D or 3-D models. We illustrate this new approximation using the electromagnetic induction response of different 3-D structures for different source fields. The QL approximation can accurately estimate the EM response for much stronger conductivity contrasts (up to hundred times) than the conventional Born approximation and over a wide range of frequencies. It also opens the possibility for fast and versatile 3-D electromagnetic inversion.

THE BORN APPROXIMATION IN 3-D EM MODELING

Consider a 3-D geoelectrical model with a normal (background) complex conductivity $\tilde{\sigma}_n$ and local inhomogeneity D, with the arbitrarily varying complex conductivity $\tilde{\sigma} = \tilde{\sigma}_n + \widetilde{\Delta\sigma}$. We will confine ourselves to consideration of nonmagnetic media and, hence, assume that $\mu = \mu_0 = 4\pi \times 10^{-7}$ *H/m,* where μ_0 is the free-space magnetic permeability. The model is excited by an electromagnetic field generated by an arbitrary source. This field is time harmonic as $e^{-i\omega t}$. Complex conductivity includes the effect of displacement currents: $\tilde{\sigma} = \sigma - i\omega\varepsilon$, where σ and ε are electrical conductivity and dielectric permittivity, respectively.

The electromagnetic fields in this model can be presented as a sum of normal and anomalous fields:

$$\mathbf{E} = \mathbf{E}^n + \mathbf{E}^a, \qquad \mathbf{H} = \mathbf{H}^n + \mathbf{H}^a, \tag{1}$$

where the normal field is a field generated by the given sources in the model with the normal distribution of conductivity $\tilde{\sigma}_n$, and the anomalous field is produced by the anomalous conductivity distribution $\Delta\tilde{\sigma}$.

It is well known that in this model the anomalous field can be presented as an integral over the excess currents in the inhomogeneous domain D (Hohmann, 1975; Weidelt, 1975; Zhdanov and Keller, 1994):

$$\mathbf{E}^a(\mathbf{r}_j) = \int\int\int_D \hat{\mathbf{G}}^n(\mathbf{r}_j|\mathbf{r})\widetilde{\Delta\sigma}(\mathbf{r})[\mathbf{E}^n(\mathbf{r}) + \mathbf{E}^a(\mathbf{r})]\, dv, \tag{2}$$

where $\hat{\mathbf{G}}^n(\mathbf{r}_j|\mathbf{r})$ is the electromagnetic Green's tensor defined for an unbounded conductive medium with the normal conductivity $\tilde{\sigma}_n$ and satisfying the equation (Zhdanov, 1988):

$$\nabla \times \nabla \times \hat{\mathbf{G}}^n(\mathbf{r}_j|\mathbf{r}) - k_n^2\hat{\mathbf{G}}^n(\mathbf{r}_j|\mathbf{r}) = -i\omega\mu_0\hat{\mathbf{I}}\delta(\mathbf{r}_j - \mathbf{r}). \tag{3}$$

Here $k_n^2 = i\omega\mu_0\tilde{\sigma}_n$, $\hat{\mathbf{I}}$ is the unit tensor, and $\delta(\mathbf{r}_j - \mathbf{r})$ is the Dirac delta function.

An integral expression for the anomalous magnetic field can be written as

$$\mathbf{H}^a(\mathbf{r}_j) = \frac{1}{i\omega\mu_0}\int\int\int_D \nabla_{r_j}\hat{\mathbf{G}}^n(\mathbf{r}_j|\mathbf{r})\widetilde{\Delta\sigma}(\mathbf{r}) \times [\mathbf{E}^n(\mathbf{r}) + \mathbf{E}^a(\mathbf{r})]\, dv. \tag{4}$$

The conventional Born approximation $E^B(r_j)$ for the anomalous field can be obtained from equation (2) if we assume that the anomalous field is negligibly small inside D in comparison with the normal field. In this case, it can be ignored in comparison with the normal field:

$$\mathbf{E}^B(\mathbf{r}_j) = \int\int\int_D \hat{\mathbf{G}}^n(\mathbf{r}_j|\mathbf{r})\widetilde{\Delta\sigma}(\mathbf{r})\mathbf{E}^n(\mathbf{r})\, dv. \tag{5}$$

Approximation (5) works reasonably well only for small conductivity contrasts between background media, a relatively small inhomogeneity, and low frequencies (Berdichevsky and Zhdanov, 1984). A detailed analysis of the range of validity of this approximation is given in (Habashy et al., 1993). In the next section, we describe the modification of the Born approximation which is similar in the basic ideas to the last one, but is much more accurate.

A QUASI-LINEAR APPROXIMATION AND THE ELECTRICAL REFLECTIVITY TENSOR

Expression (2) can be rewritten using operator notations:

$$\mathbf{E}^a = \mathbf{C}[\mathbf{E}^a], \tag{6}$$

where $C[E^a]$ is an integral operator of the anomalous field E^a

$$\mathbf{C}[\mathbf{E}^a] = \mathbf{A}[\mathbf{E}^n] + \mathbf{A}[\mathbf{E}^a] \tag{7}$$

and A is a linear scattering operator:

$$\mathbf{A}[\mathbf{E}] = \int\int\int_D \hat{\mathbf{G}}^n(\mathbf{r}_j|\mathbf{r})\widetilde{\Delta\sigma}(\mathbf{r})\mathbf{E}(\mathbf{r})\, dv. \tag{8}$$

Equation (6) can be treated as an integral equation with respect to the anomalous field E^a. The solution of this integral equation has to be a fixed point of the operator C (in other words, the application of the operator C to the anomalous field E^a does not change this field). This solution can be obtained using the method of successive iterations that is governed by the equations

$$\mathbf{E}^{a(N)} = \mathbf{C}[\mathbf{E}^{a(N-1)}], \quad N = 1, 2, 3, \ldots \tag{9}$$

It is well known that successive iterations converge if operator C is a contraction operator (Banach theorem), that is

$$\|\mathbf{C}[\mathbf{E}^{a(1)} - \mathbf{E}^{a(2)}]\| \le k\|\mathbf{E}^{a(1)} - \mathbf{E}^{a(2)}\|, \tag{10}$$

where $\|\cdots 11$ is L_2 norm, $k < 1$, and $E^{a(1)}$ and $E^{a(2)}$ are any two different solutions. Substituting (7) into (10) we obtain

$$\|\mathbf{C}[\mathbf{E}^{a(1)} - \mathbf{E}^{a(2)}]\| = \|\mathbf{A}[\mathbf{E}^{a(1)} - \mathbf{E}^{a(2)}]\|$$
$$\le \|\mathbf{A}\|\,\|\mathbf{E}^{a(1)} - \mathbf{E}^{a(2)}\|. \tag{11}$$

Therefore, condition (10) holds if $\|\mathbf{A}\| < 1$.

If operator C is a contraction, then the Nth iteration approaches the actual anomalous field

$$\mathbf{E}^{a(N)} \to \mathbf{E}^{a}, \tag{12}$$

when $N \to \infty$.

The Born approximation is simply the first iteration of this method, if the initial approximation $E^{a(0)}$ (zero order iteration) is selected to be equal to zero ($E^{a(0)} = 0$):

$$E^{B} = E^{a(1)} = C[0] = A[E^{n}]. \tag{13}$$

In this case the Nth iteration can be treated as the sum of N terms of the Neumann (or Born) series:

$$Ea^{(N)} = AE^{n} + A^{2}E^{n} + A^{3}E^{n} + \ldots + A^{N}E^{n}$$
$$= E^{B} + A^{2}E^{n} + A^{3}E^{n} + 111 + A^{N}E^{n}. \tag{14}$$

We will obtain a more accurate approximation if we assume that the anomalous field E^{a} inside the inhomogeneous domain is not equal to zero, but is linearly related to the normal field E^{n} by some tensor $\hat{\lambda}$:

$$E^{a}(r) \approx \hat{\lambda}(\mathbf{r})\mathbf{E}^{n}(\mathbf{r}). \tag{15}$$

By analogy with the geoelectrical reflection coefficients for the layered models (Zhdanov and Keller, 1994) and with the seismic case (Bleistein, 1984), we will call $\hat{\lambda}(\mathbf{r})$ an *electrical reflectivity tensor.*

Subsequently, we use the expression (15) as the zero-order approximation for the scattered field inside the inhomogeneity ($E^{a(0)} = \hat{\lambda}\mathbf{E}^{n}$) and calculate the first approximation as

$$E^{a(1)} = \mathbf{C}[\hat{\lambda}\mathbf{E}^{n}] = A[E^{n} + \hat{\lambda}\mathbf{E}^{n}] = \mathbf{A}[(\hat{\mathbf{I}} + \hat{\lambda})\mathbf{E}^{n}]. \tag{16}$$

We will call this approximation a *quasi-linear (QL) approximation* $\mathbf{E}^{a}_{q\ell}$ for the anomalous field because it generates an integral expression for the scattered field which is nonlinear with respect to the conductivity (the reflectivity tensor $\hat{\lambda}$ is in the general case a function of $\Delta\bar{\sigma}$ as well), but which is linear with respect to the product of conductivity and reflectivity tensor. Taking into account (8) we have

$$\mathbf{E}^{a}_{q\ell} = \mathbf{E}^{a(1)} = \iiint_{D} \hat{\mathbf{G}}^{n}(\mathbf{r}_j|\mathbf{r})\,\bar{\Delta}\sigma(\mathbf{r})[\hat{\mathbf{I}} + \hat{\lambda}(\mathbf{r})]\mathbf{E}^{n}(\mathbf{r})\,dv. \tag{17}$$

Up till now the background of the Born approximation and new QL approximation is the same. The main difference is that in the case of the Born approximation the starting point for the iteration process is the zero scattered field, while in our approach we start with the scattered field proportionate (in an as yet arbitrary way) to the normal field. In principle, we can expand our approach to computing all iterations by equation (9). In this case we will obtain a complete analog of the Born series. However, in this paper we will analyze only the first QL approximation.

Let us estimate an accuracy of the QL approximation. According to equations (6) and (7) the actual anomalous field E^{a} is equal to

$$E^{a} = A[E^{n}] + A[E^{a}]. \tag{18}$$

Comparing E^{a} with the QL approximation, we can obtain an accuracy criterion for a QL solution:

$$\|\mathbf{E}^{a} - \mathbf{E}^{a}_{q\ell}\| = \|\mathbf{A}(\mathbf{E}^{a} - \hat{\lambda}\mathbf{E}^{n})\| \le \|\mathbf{A}\|\,\|\mathbf{E}^{a} - \hat{\lambda}\mathbf{E}^{n}\|. \tag{19}$$

Equation (19) shows that the accuracy of the QL approximation depends on the accuracy $\delta = \|\mathbf{E}^{a} - \hat{\lambda}\mathbf{E}^{n}\|$ of equation (15):

$$\|\mathbf{E}^{a} - \mathbf{E}^{a}_{q\ell}\| \le \|\mathbf{A}\|\delta. \tag{20}$$

Taking into account that the electrical reflectivity tensor $\hat{\lambda}(\mathbf{r})$ is, in the general case, a function of the observation point r, it is clear that δ can be made arbitrarily small if $\hat{\lambda}(\mathbf{r})$ is closely specified.

At this point it is interesting to analyze the difference between a QL approximation and the second-order Born approximation that is given according to equation (14) by the formula

$$\mathbf{E}^{a(2)} = \mathbf{A}\mathbf{E}^{n} + \mathbf{A}^{2}\mathbf{E}^{n} = \mathbf{A}[\mathbf{E}^{n} + \mathbf{A}\mathbf{E}^{n}] \tag{21}$$

Comparing equations (16) and (21), we see that the QL approximation can be obtained formally from the second-order Born approximation if we substitute operator A within the square brackets in equation (21) by the electrical reflectivity tensor $\hat{\lambda}$. However, these two approximations are different because we have a choice in the selection of the tensor $\hat{\lambda}$, and, therefore, we can obtain the better approximation for the anomalous field. The main problem is to find the corresponding tensor function $\hat{\lambda}(\mathbf{r})$ that would minimize δ.

Our approach to the solution of this problem will be based on the following analysis. Using equation (16) we can express $\|\mathbf{E}^{a} - \hat{\lambda}\mathbf{E}^{n}\|$ as follows:

$$\|\mathbf{E}^{a} - \hat{\lambda}\mathbf{E}^{n}\| = \|\mathbf{E}^{a} - \mathbf{E}^{a}_{q\ell} + \mathbf{A}[(\hat{\mathbf{I}} + \hat{\lambda})\mathbf{E}^{n}] - \hat{\lambda}\mathbf{E}^{n}\|$$
$$\le \|\mathbf{E}^{a} - \mathbf{E}^{a}_{q\ell}\| + \|\mathbf{A}[(\hat{\mathbf{I}} + \hat{\lambda})\mathbf{E}^{n}] - \hat{\lambda}\mathbf{E}^{n}\|. \tag{22}$$

Let us determine $\hat{\lambda}$ from the condition

$$\|\mathbf{A}[(\hat{\mathbf{I}} + \hat{\lambda}) \cdot \mathbf{E}^{n}] - \hat{\lambda} \cdot \mathbf{E}^{n}\| = \varphi(\hat{\lambda}) = \min. \tag{23}$$

From inequalities (19) and (22) we have

$$\|\mathbf{E}^{a} - \mathbf{E}^{a}_{q\ell}\| \le \|\mathbf{A}\|\{\|\mathbf{E}^{a} - \mathbf{E}^{a}_{q\ell}\| + \varphi(\hat{\lambda})\}. \tag{24}$$

In the beginning of this section we stated that in order for the Born series expansion to converge to the actual electric field, the condition

$$\|\mathbf{A}\| < 1 \tag{25}$$

is required. Under this condition we can rewrite inequality (24) as

$$\|\mathbf{E}^{a} - \mathbf{E}^{a}_{q\ell}\| \le \frac{\|\mathbf{A}\|}{1 - \|\mathbf{A}\|}\,\varphi(\hat{\lambda}). \tag{26}$$

The last formula shows that the minimum of equation (23) determines the accuracy of the QL approximation.

Note that the electrical reflectivity tensor $\hat{\lambda}$ is formally connected with the scattering tensor $\hat{\Gamma}$, introduced in Habashy et al., 1993, by the simple formula

$$\hat{\lambda} = \hat{\mathbf{\Gamma}} - \hat{\mathbf{I}}. \tag{27}$$

However, Torres-Verdin and Habashy use a quasi-analytical expression to determine $\hat{\Gamma}$ while we will use condition (23) for the numerical calculation of the electrical reflectivity tensor. This numerical approach opens a way to impose additional restrictions on the reflectivity tensor.

For example, we can demand that $\hat{\lambda}$ is a diagonal tensor:

$$\hat{\lambda} = \begin{bmatrix} \lambda_x & 0 & 0 \\ 0 & \lambda_y & 0 \\ 0 & 0 & \lambda_z \end{bmatrix}. \tag{28}$$

In other words, we can assume that every componetn of the anomalous field is linearly proportionate to the component of normal field along the same axes.

Alternatively,

$$\hat{\lambda} = \lambda \hat{\mathbf{I}}. \tag{29}$$

Of course, these assumptions make our approximate solution less accurate. However, as we will see below, in some situations they work very well.

DETERMINATION OF THE REFLECTIVITY TENSOR

In this section, we develop the numerical method for the electrical reflectivity tensor estimation in complicated models. To solve this problem we rewrite equation (17) for the points inside domain *D,* taking into account equation (15):

$$\mathbf{E}^a_{q\ell} \approx \hat{\lambda}\mathbf{E}^n \approx \mathbf{A}[(\hat{\mathbf{I}} + \hat{\lambda})\mathbf{E}^n]$$

$$= \int\int\int_D \hat{\mathbf{G}}^n(\mathbf{r}_j|\mathbf{r})\tilde{\Delta\sigma}(\mathbf{r})[\hat{\mathbf{I}} + \hat{\lambda}(\mathbf{r})]\mathbf{E}^n(\mathbf{r})\, dv. \tag{30}$$

The last equation provides the basis for determining $\hat{\lambda}$. This equation should hold for any internal point of the domain *D.* In reality, of course, it holds only approximately. Therefore we can use the minimum norm condition to determine $\hat{\lambda}$:

$$\left\| \hat{\lambda}(\mathbf{r}_j)\mathbf{E}^n(\mathbf{r}_j) - \int\int\int_D \hat{\mathbf{G}}^n(\mathbf{r}_j|\mathbf{r})\tilde{\Delta}\sigma(\mathbf{r})[(\hat{\mathbf{I}} + \hat{\lambda})\mathbf{E}^n(\mathbf{r})]\, dv \right\|$$

$$= \varphi(\hat{\lambda}) = \min. \tag{31}$$

As we mentioned in the previous section, the electrical reflectivity tensor $\hat{\lambda}$ is connected with the scattering tensor $\hat{\mathbf{\Gamma}}$ introduced in Habashy et al., 1993 by the simple formula (27). Therefore, we can use some results obtained in Habashy et al. (1993) for the scattering tensor to analyze the properties of the reflectivity tensor. First of all, we can assume that the reflectivity tensor $\hat{\lambda}$, like $\hat{\mathbf{\Gamma}}$, reflects the conductivity distribution. Also this approximation is valid under the assumption that the internal field, and therefore the reflectivity tensor, is varying slowly inside the inhomogeneous domain (Torres-Verdin and Habashy, 1994). The correctness of this assumption can be illustrated by numerical calculations.

Consider the 3-D geoelectrical model consisting of a homogeneous half-space (with resistivity 100 ohm l m) and a conductive rectangular inclusion with a resistivity of 1 ohm l m (Figure 1). The electromagnetic field in the model is excited by a horizontal rectangular loop, located 50 m to the left of the model, with the loop 10 m on a side and the current at 1 A. We have used the integral equation program SYSEM for computing the frequency-domain response of the complex conductivity structure (Xiong, 1992). This code makes it possible to calculate the EM field not only on the surface of observation, but inside the conductive half-space. For the sake of simplicity we assume also that the reflectivity tensor is diagonal, as in equation (28). After defining the normal and anomalous fields in the conductive half-space by forward modeling, we have used equation (15) to compute all of the components of the diagonal reflectivity tensor for different frequencies. Calculations have been done for the receivers, located along the profile AB crossing the top of the conducting body (Figure 1). The plot of the λ_x component at the frequency $f = \omega/2\pi =$ 1 Hz is shown on Figure 2. One can see that λ_x changes rapidly outside the body, but is almost constant inside the body (about 400 cells were used for sampling λ_x inside the body). The same results have been obtained for other components of $\hat{\lambda}$ and frequencies between 0.001 Hz and 1000 Hz. Models with conductive inclusions of $\rho_2 = 10$ ohm l m and $\rho_2 = 0.1$ ohm l m produce the same results. Moreover, calculations show that the value of λ_x is constant everywhere inside the conducting body. For example, Figure 3 presents the plot of λ_x for the vertical cross-sectionx = 0 for 10 Hz. Figure 4 presents the same plot at the vertical cross-section $x = 2.5$ m and for 1000 Hz. The white zones on these figures delineate the anomalous body very well. Thus, our assumption about the slow variation of λ_x inside the anomalous domain is correct. The problem is how to determine the tensor $\hat{\lambda}$.

For the numerical calculation, it is more convenient to rewrite equation (30) using tensor notations

$$E^a_{q\ell\alpha}(\mathbf{r}_j) \approx \lambda_{\beta\gamma}\delta_{\alpha\beta}E^n_\gamma(\mathbf{r}_j)$$

$$\approx \int\int\int_D G^n_{\alpha\beta}(\mathbf{r}_j|\mathbf{r})\tilde{\Delta\sigma}(\mathbf{r})[\delta_{\beta\gamma} + \lambda_{\beta\gamma}(\mathbf{r})]E^n_\gamma(\mathbf{r})\, dv;$$

$$\alpha, \beta, \gamma = x, y, z. \tag{32}$$

In the last equation, $E^a_{q\ell\alpha}(\mathbf{r})$ and $E^n_\gamma(\mathbf{r})(\alpha, \gamma = x, y, z)$ are the Cartesian components of the electric field vectors, and $G^n_{\alpha\beta}(\mathbf{r}_j|\mathbf{r})$, $\alpha, \beta = x, y, z$ are the Cartesian components of the electromagnetic Green's tensor. In all equations with summations we use the *Einstein convention:* the twice recurring index indicates summation over this index (for example, $\beta = x, y, z$).

Following our assumption about slow variation of the tensor $\hat{\lambda}$ inside the anomalous domain, we begin our analysis with the simplest case of the constant reflectivity tensor inside *D.* Therefore, equation (32) takes the form

$$E^a_\alpha(\mathbf{r}_j) \approx \lambda_{\beta\gamma}\delta_{\alpha\beta}E^n_\gamma(\mathbf{r}_j) \approx (\delta_{\beta\gamma} + \lambda_{\beta\gamma})$$

$$\times \int\int\int_D G^n_{\alpha\beta}(\mathbf{r}_j|\mathbf{r})\tilde{\Delta\sigma}(\mathbf{r})\; E^n_\gamma(\mathbf{r})\, dv, \tag{33}$$

and we have

$$\lambda_{\beta\gamma}\left[\delta_{\alpha\beta}E^n_\gamma(\mathbf{r}_j) - \int\int\int_D G^n_{\alpha\beta}(\mathbf{r}_j|\mathbf{r})\tilde{\Delta\sigma}(\mathbf{r})E^n_\gamma(\mathbf{r})\,dv\right] \approx E^B_\alpha(\mathbf{r}_j), \quad (34)$$

where $\mathbf{r}_j \in D$.

This equation, as well as relationship (30) holds only approximately. Therefore we can use the least-squares method to determine the $\hat{\lambda}$ that optimally fits condition (34):

$$\varphi(\hat{\lambda}) = \sum_{j=1}^{J}[E^B_\alpha(\mathbf{r}_j) - \lambda_{\beta\gamma}\Delta E_{\alpha\beta\gamma}(\mathbf{r}_j)]^* \times [E^B_\alpha(\mathbf{r}_j) - \lambda_{\mu\nu}\Delta E_{\alpha\mu\nu}(\mathbf{r}_j)] = \min; \quad \alpha, \beta, \gamma, \mu, \nu = x, y, z; \quad (35)$$

where $\Delta E_{\alpha\beta\gamma}$ is the bracketed term in equation (34):

$$\Delta E_{\alpha\beta\gamma}(\mathbf{r}_j) = \delta_{\alpha\beta}E^n_\gamma(\mathbf{r}_j) - \int\int\int_D G^n_{\alpha\beta}(\mathbf{r}_j|\mathbf{r})\tilde{\Delta\sigma}(\mathbf{r})E^n_\gamma(\mathbf{r})\,dv, \quad (36)$$

and the superscript * means the complex conjugate value.

The solution of the minimization problem (35) is described in Appendix A. The components of the optimal reflectivity tensor are

$$[\lambda_{\mu\nu}] = \left[\sum_{j=1}^{J}\Delta E^*_{\alpha\beta\gamma}(\mathbf{r}_j)\Delta E_{\alpha\mu\nu}(\mathbf{r}_j)\right]^{-1} \times \left[\sum_{j=1}^{J}\Delta E^*_{\alpha\beta\gamma}(\mathbf{r}_j)E^B_\alpha(\mathbf{r}_j)\right]. \quad (37)$$

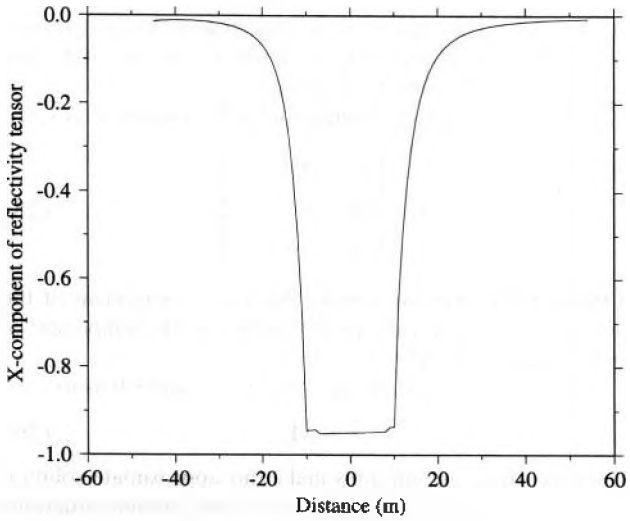

FIG. 2. Plot of the A, component of the reflectivity tensor computed for Model 1 at frequency f = $\omega/2\pi$ = 1 Hz. Calculations have been done for the receivers located along profile AB crossing the conducting body at its top side (see Figure 1). A, changes rapidly outside the body, but is almost constant inside the body (- 10 ≤ y ≤ 10).

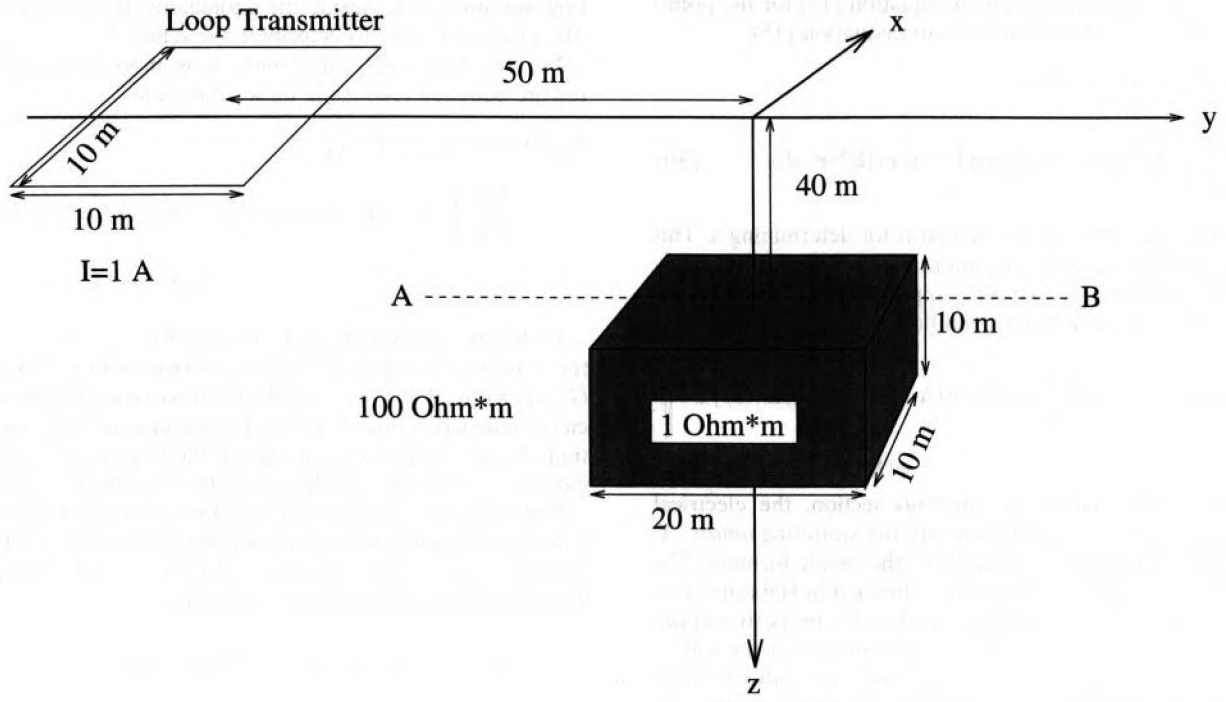

Model 1

FIG. 1. 3-D geoelectric model, containing one conductive body in a homogeneous half-space, with rectangular loop excitation (Model 1). AB is a profile of receivers.

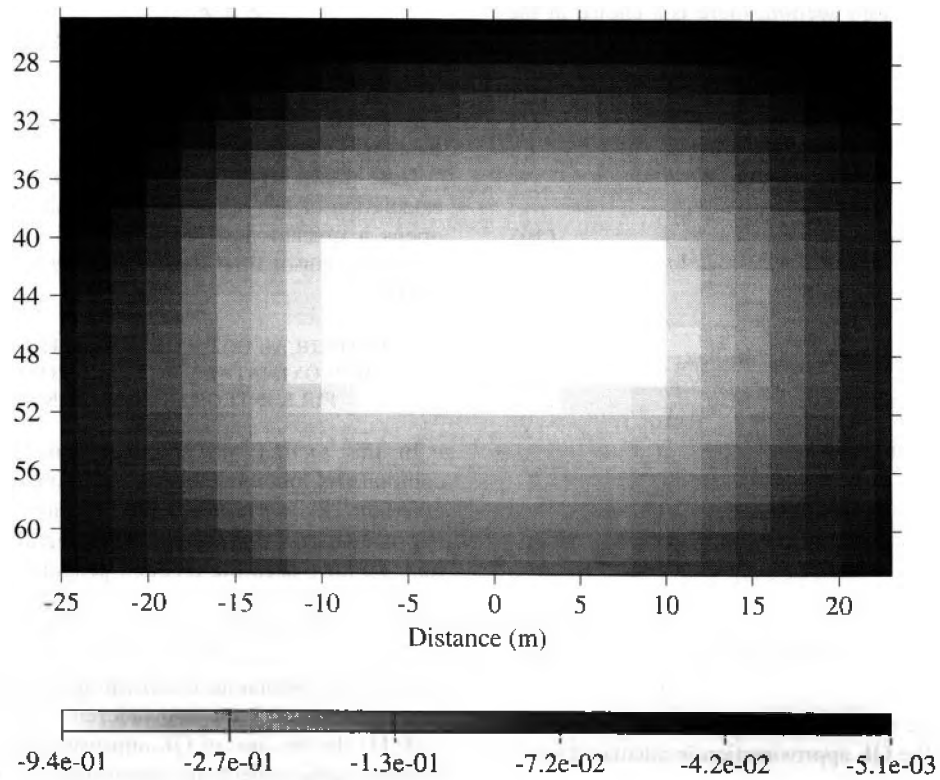

FIG. 3. Plot of the real part of component λ_x at the vertical cross-section $x = 0$ of the reflectivity tensor, computed for Model 1 (Figure 1) at frequency $f = \omega/2\pi = 10$ Hz (the imagina part of λ_x is negligibly small). White and black scale represents the dimensionless values of A,. The white domain corresponds to the constant value of A,. This white domain coincides with the geometry of the anomalous body.

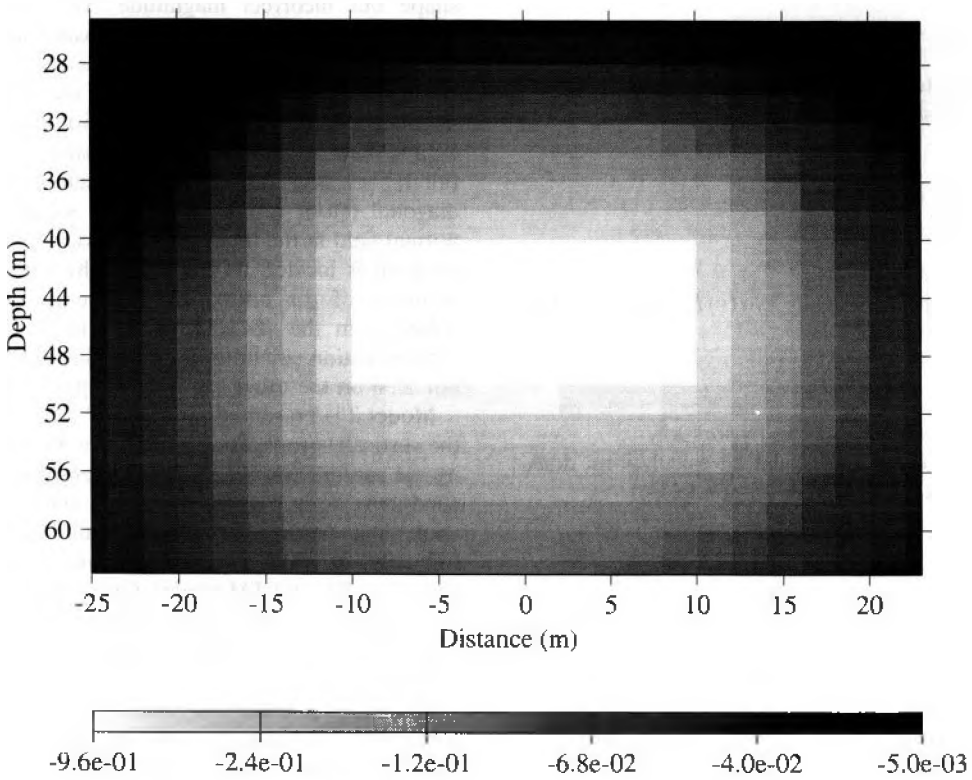

FIG. 4. Plot of the real part of the component A, at the vertical cross-section $x = 2.5$ m of the reflectivity tensor, computed for Model 1 (Figure 1) at frequency $f = \omega/2\pi = 1000$ Hz (the imaginary part of A, is negligibly small). The white domain corresponds to the constant value of A,. This white domain coincides with the geometry of the anomalous body.

As we noted in the previous section, there is a choice in the selection of the type of the electrical reflectivity tensor. For example, in the simplest case when $\hat{\lambda}$ is a scalar tensor

$$\lambda_{\beta\gamma} = \lambda\delta_{\beta\gamma} \tag{38}$$

we obtain

$$\lambda = \frac{\sum_{j=1}^{J} \Delta E^{*}_{\alpha\beta\beta}(\mathbf{r}_j) E^{B}_{\alpha}(\mathbf{r}_j)}{\sum_{j=1}^{J} \Delta E^{*}_{\alpha\beta\beta}(\mathbf{r}_j) \Delta E_{\alpha\mu\mu}(\mathbf{r}_j)}. \tag{39}$$

In the case when $\hat{\lambda}$ is a diagonal tensor

$$\lambda_{\beta\gamma} = \begin{cases} \lambda_{\beta}, \ \beta = \gamma = x, y, z \\ 0, \ \beta \neq \gamma \end{cases}, \tag{40}$$

the solution has the form

$$[\lambda_{\mu}] = \left[\sum_{j=1}^{J} \Delta E^{*}_{\alpha\beta}(\underline{\mathbf{r}}_j) \Delta E_{\alpha\mu}(\mathbf{r}_j) \right]^{-1} \times \left[\sum_{j=1}^{J} \Delta E^{*}_{\alpha\beta}(\underline{\mathbf{r}}_j) E^{B}_{\alpha}(\underline{\mathbf{r}}_j) \right]. \tag{41}$$

In the general case we should solve equation (37) to find λ. After the $\hat{\lambda}$ is found, the QL approximation is calculated using expression (17).

We can obtain a more precise approximation for the electric field if we divide the domain D into subdomains $D = \cup_{k=1,K} D_k$ and assume that relationship (30) holds inside any subdomain *Dk:*

$$E^{a}_{\beta}(\mathbf{r}_j) = \lambda^{k}_{\beta\gamma} E^{n}_{\gamma}(\mathbf{r}_j), \ \mathbf{r}_j \in D_k, \tag{42}$$

where the reflectivity tensor $\lambda^{k}_{\beta\gamma}$ depends only on the subdomain's number *k*. Substituting equation (42) into equation (2) we have

$$\lambda^{m}_{\beta\gamma}\delta_{\alpha\beta} E^{n}_{\gamma}(\mathbf{r}_j) \approx \sum_{k=1,K} (\delta_{\beta\gamma} + \lambda^{k}_{\beta\gamma}) \times \int\int\int_{D} G^{n}_{\alpha\beta}(\mathbf{r}_j|\mathbf{r}) \widetilde{\Delta\sigma}(\mathbf{r}) \ E^{n}_{\gamma}(\mathbf{r}) \ dv, \tag{43}$$

$$\mathbf{r}_j \in D_m.$$

Now the problem is to determine the tensors $\hat{\lambda}^{k}$.

To solve this problem we can repeat all calculations, done above for one constant tensor $\hat{\lambda}$ (see Appendix B).

Thus, we obtain

$$[\lambda^{m}_{\mu\nu}] = \left[\sum_{j=1}^{J} \Delta E^{*}_{\alpha\beta\gamma k}(\mathbf{r}_j) \Delta E_{\alpha\mu\nu m}(\mathbf{r}_j) \right| \times \left[\sum_{j=1}^{J} \Delta E^{*}_{\alpha\beta\gamma k}(\mathbf{r}_j) E^{B}_{\alpha}(\mathbf{r}_j) \right], \tag{44}$$

where

$$\mathrm{AE}_{\alpha\beta\gamma k}(\mathbf{r}_j) = \delta_{\alpha\beta}\delta_{k\ell} E^{n}_{\gamma}(\mathbf{r}_j) - \int\int\int_{D_k} G^{n}_{\alpha\beta}(\mathbf{r}_j|\mathbf{r}) \widetilde{\Delta\sigma}(\mathbf{r}) \ E^{n}_{\gamma}(\mathbf{r}) \ dv. \tag{45}$$

The last expression also can be simplified for the cases of diagonal or scalar reflectivity tensor.

Note that, according to equation (27), the method of calculation of the reflectivity tensor developed in this section opens a quicker and more efficient way of arriving at the scattering tensor than is given in Torres-Verdin and Habashy (1994).

NUMERICAL COMPARISON OF THE QUASI-LINEAR APPROXIMATION, BORN APPROXIMATION, AND FULL INTEGRAL EQUATION SOLUTIONS

In this section, we compare numerically the EM field components, obtained by the solution of the exact integral equation (2), the Born approximation (5) and the linear approximation (17). For the full integral equation (IE) solution, we have used the SYSEM program (Xiong, 1992).

First, we analyze the results of the numerical calculation for model 1, presented in Figure 1. Figures 5 and 6 show the comparison of the different solutions for real and imaginary parts of the anomalous electrical field E^{a}_{x} and the anomalous magnetic field H^{a}_{z} for two different frequencies: 10 Hz and 1000 Hz. In the case of QL approximation, we have used the simplest scalar reflectivity tensor and the diagonal reflectivity tensor. One can see that the full solution and the QL approximations calculated with the use of the scalar and the diagonal reflectivity tensor produce similar results, while the conventional Born approximation produces curves of the correct shape but incorrect magnitude. We can observe a small difference between the QL approximations and a full IE solution only on the ReH^{a}_{z} component near the center of the body. Notice, that the symmetry in the absolute value of the anomalous field, observed on the Born approximation and QL approximation computed with the scalar $\hat{\lambda}$, is destroyed for the full IE solution and QL approximation computed with the diagonal tensor $\hat{\lambda}$. This fact has a simple explanation. The normal field in the model is asymetrical because the transmitter loop is located to the left of the conducting body. This asymetry of the normal field generates the same type of asymetry in the IE solution and in the more precise QL approximation computed with the diagonal tensor $\hat{\lambda}$, and it is not seen on the other less precise approximations.

Model 2 is presented on Figure 7. This model is excited by the vertically propagating plane wave. For the sake of symplicity, we assume that the reflectivity tensor is a scalar inside the conductive body. Figure 8 compares different solutions for the anomalous fields ReH^{a}_{x}, ReH^{a}_{y} and ReE^{a}_{x}, ImE^{a}_{y} for a frequency of 1 Hz. Figure 9 presents the apparent resistivity curves for TE and TM modes. One can see again that the full solution and the QL approximation produce similar results, and that the Born approximation lies far away from the exact solution.

Model 3 contains two anomalous bodies with different resistivities-1 ohm l m and 100 ohm · m-immersed in a three-layer earth (Figure 10). We again consider plane-wave excitation and assume that the reflectivity tensor is scalar within every body, but a different function for conductive (1 ohm l m) and resistive (100 ohm l m) inclusions. Results of

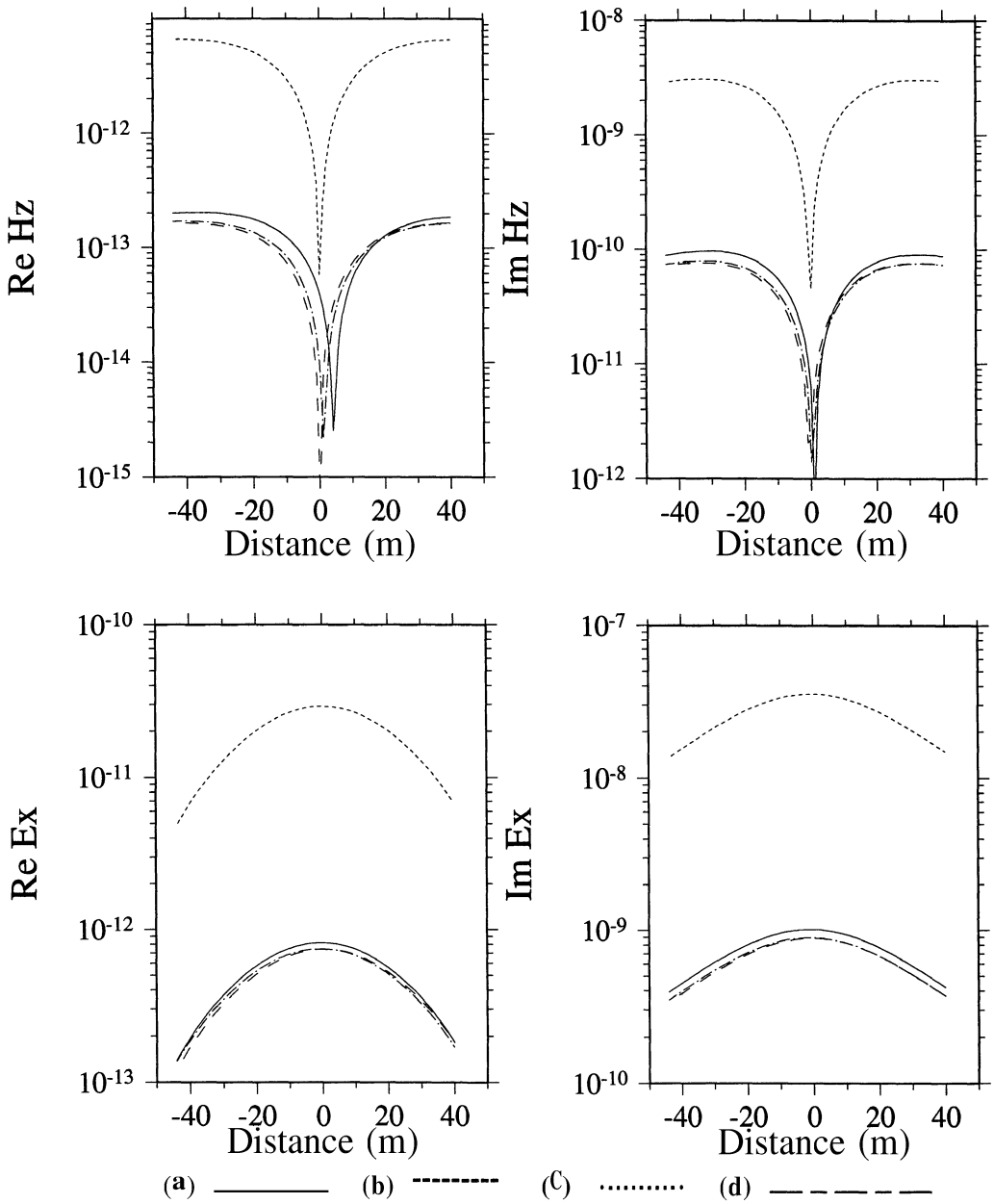

FIG. 5. Numerical corn arison of full IE solution (a), QL approximation with the use of the scalar electrical reflectivity tensor (b), Born approximation (c),and QL approximation with the use of the diagonal electrical reflectivity tensor (d) computed for Model 1 (Figure 1) at the frequency $f = \omega/2\pi =$ 10 Hz. Calculations done for the receivers located along the Y-axis on the surface. Real and imaginary components of electric and magnetic fields are presented.

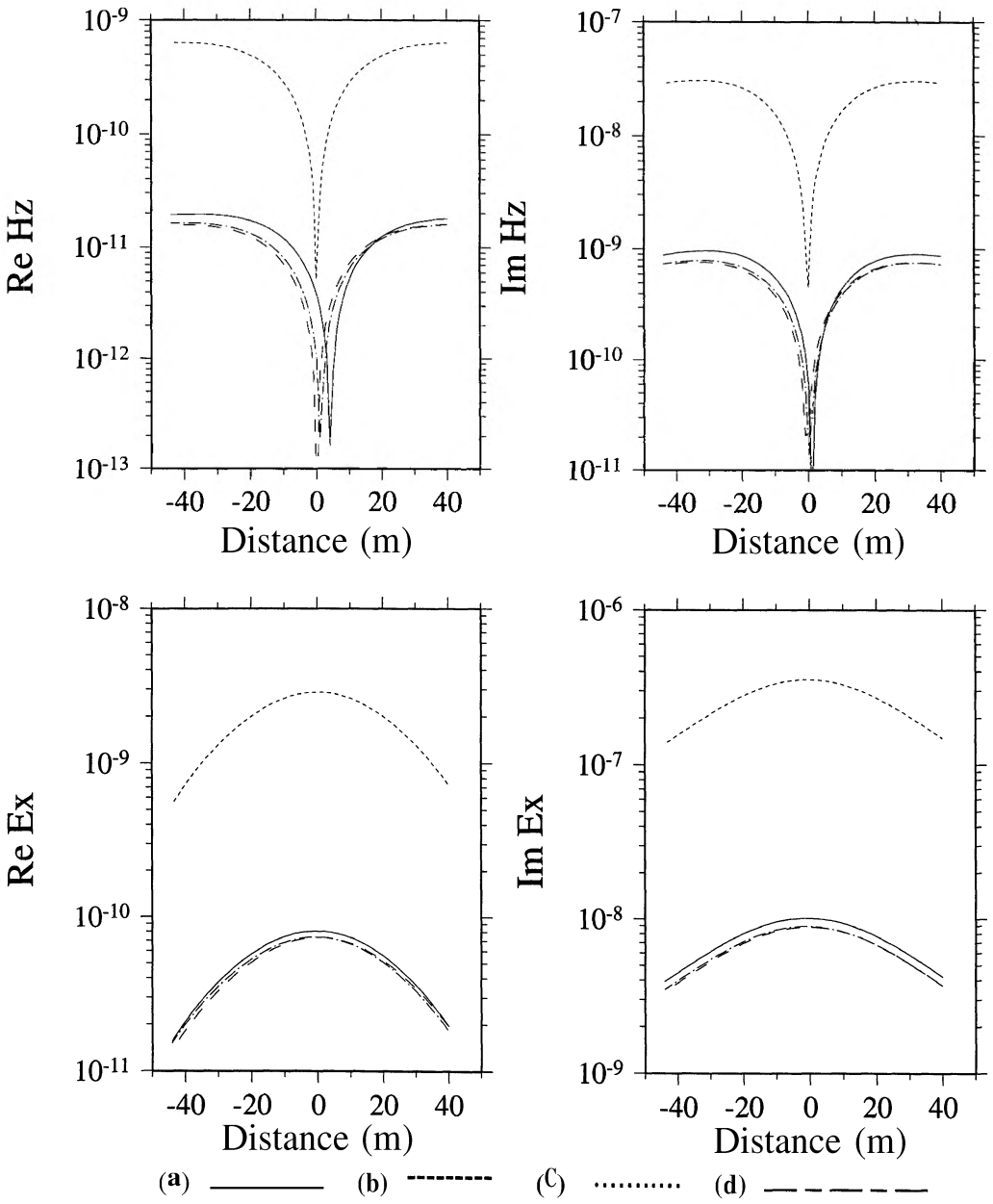

FIG. 6. Numerical comparison of full IE solution (a), QL approximation with the use of the scalar electrical reflectivity tensor (b), Born approximation (c), and QL approximation with the use of the diagonal electrical reflectivity tensor (d) computed for Model 1 (Figure 1) at the frequency $f = \omega/2\pi =$ 1000 Hz. Calculations are done for the receivers located along the Y-axis on the surface. Plots present real and imaginary components of the electric and magnetic fields.

numerical EM modeling are presented in Figure 11 (anomalous field components) and Figure 12 [apparent resistivity curves for transverse electric (TE) and transverse electric (TM) modes]. The conclusion of the analysis of these results is the same: the full solution and the QL approximation produce similar results, while the Born approximation generates an erroneous solution.

The last model, model 4, with three conductive bodies is shown in Figure 13. This model simulates the VLF observations: we have a shallow conductive structure and consider high-frequency plane-wave excitation-up to 500 kHz. The reflectivity tensor is scalar and could be equal to different functions for different bodies:

$$\hat{\lambda}^k = \lambda^{(k)}\hat{\mathbf{I}}, \quad k = 1, 2, 3.$$

Results of numerical modeling are presented in Figures 14 and 15. The conclusion is the same as for the previous models: a QL approximation works well while the Born approximation does not.

It is important to compare the computational time of the numerical modeling needed for any of these three approaches. The results of comparison are presented in Tables 1 and 2.

One can see from these tables that CPU time increases exponentially with the number of cells for a full IE solution, while it increases linearly for the QL approximation and Born approximation. In the models with 800 cells in the anomalous domain, the QL approximation is an order of magnitude faster than the full IEs solution. It takes about twice the time to compute the QL approximation that is required for Born approximation. However, the QL approximation produces reasonable results, while the Born approximation gives a poor estimate.

CONCLUSION

The QL approximation of the EM field developed in this paper is based on the approximation of the anomalous field by a linear transformation of the normal field: $\mathbf{E}_a = \hat{\lambda}\mathbf{E}_n$, where $\hat{\lambda}$ is called the *electrical reflectivity tensor*. The reflectivity tensor inside inhomogeneities can be approximated by slow varying functions that can be determined numerically by a simple optimization technique.

The results of numerical calculations have shown that the new approximation gives an accurate estimate of the 3-D EM response for a much stronger conductivity contrast (up to hundred times) than does the conventional Born approximation and for a wide range of frequencies. At the same time, this method is much faster than the computer codes based on the full IE solution. Thus it opens up a possibility for fast 3-D electromagnetic inversion.

ACKNOWLEDGMENTS

We thank the Consortium on Electromagnetic Modeling and Inversion (CEMI) at the Department of Geology and Geophysics, University of Utah, for providing support for this work. We wish to thank Dr. Z. Xiong for help in the work with his 3-D integral equation code and Dr. Al Tripp for useful discussions and comments.

(Continued on p. 663)

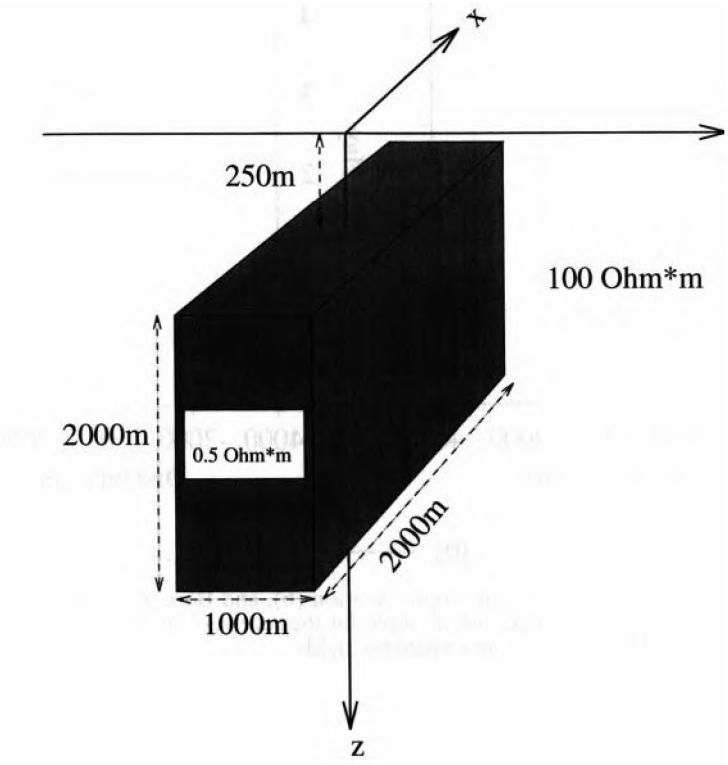

Model 2

FIG. 7.3-D geoelectric model containing one conductive body in a homogeneous half-space with a plane-wave excitation (Model 2).

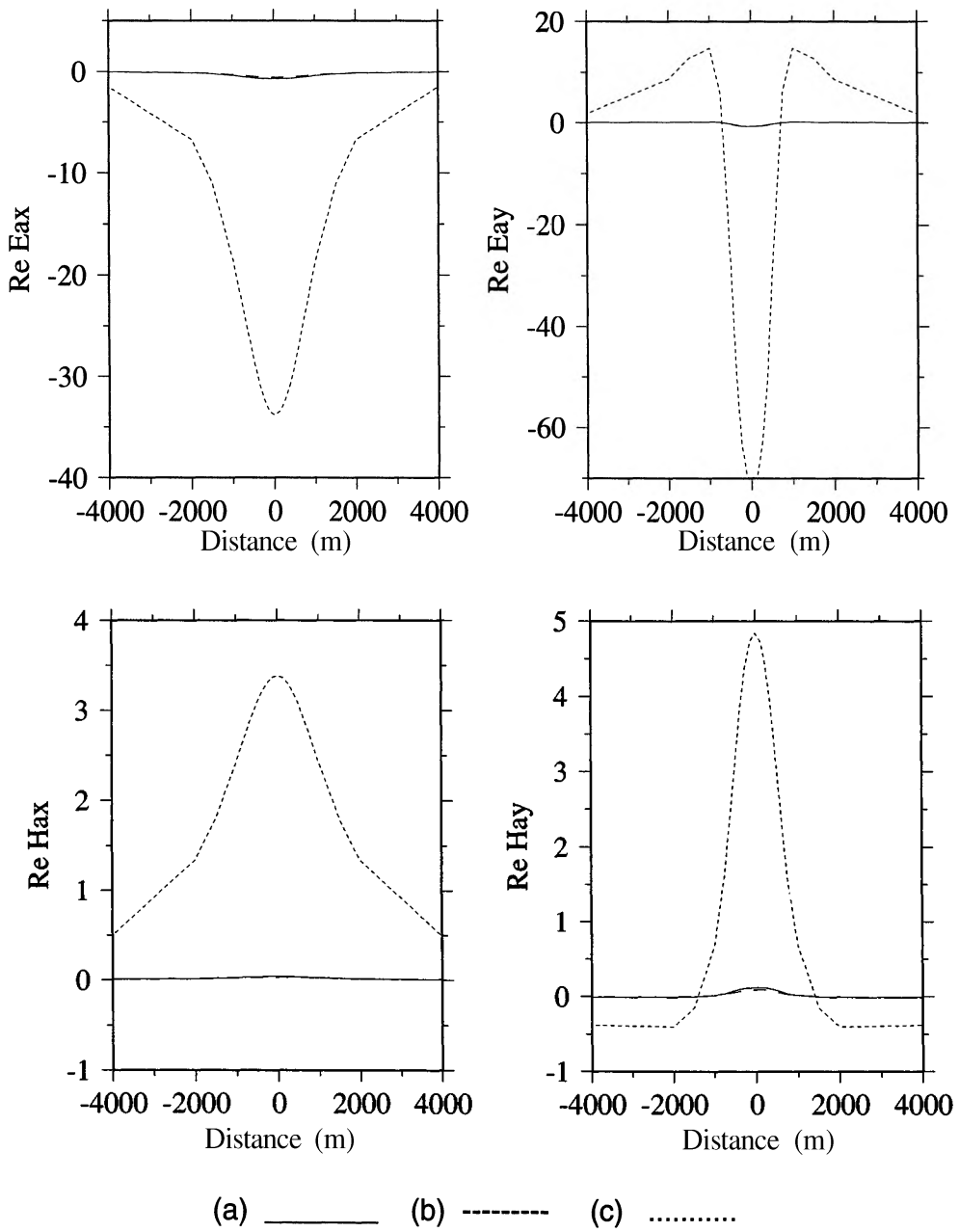

FIG. 8a. Numerical comparison of full IE solution (a , QL approximation (b), and Born approximation (c) computed for Model 2 (Figure 7) at the frequency $f = \omega/2\pi = 1$ Hz. Calculations are done for the receivers located along the Y-axis on the surface. Plots present real and imaginary components of the electric and magnetic fields.

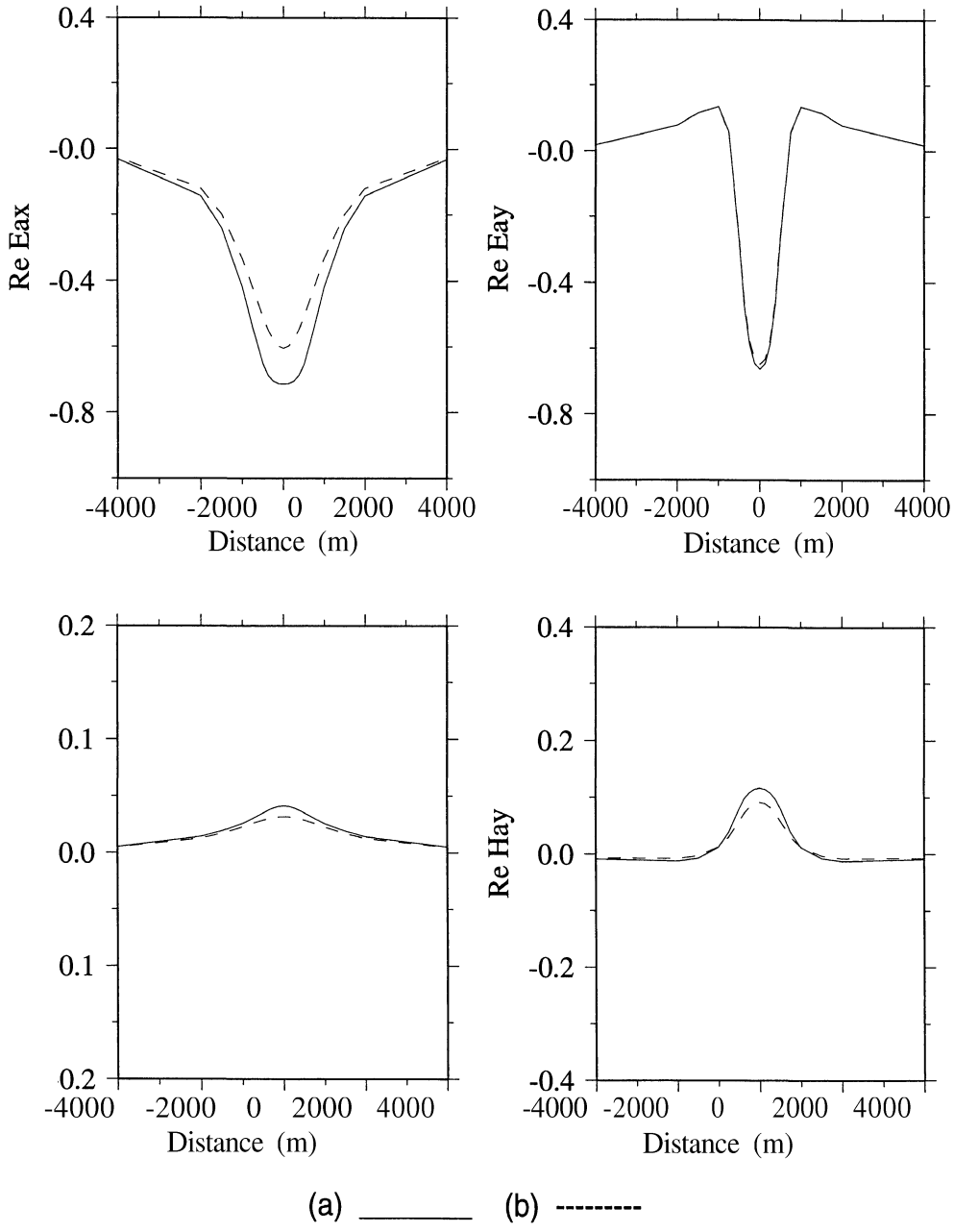

FIG. 8b. Numerical comparison of full IE solution (a) and QL approximation (b) computed for Model 2 (Figure 7) at the frequency $f = \omega/2\pi = 1$ Hz. Calculations are done for the receivers located along the Y-axis on the surface. Plots present real and imaginary components of the electric and magnetic fields for a larger vertical scale than in Figure 8a.

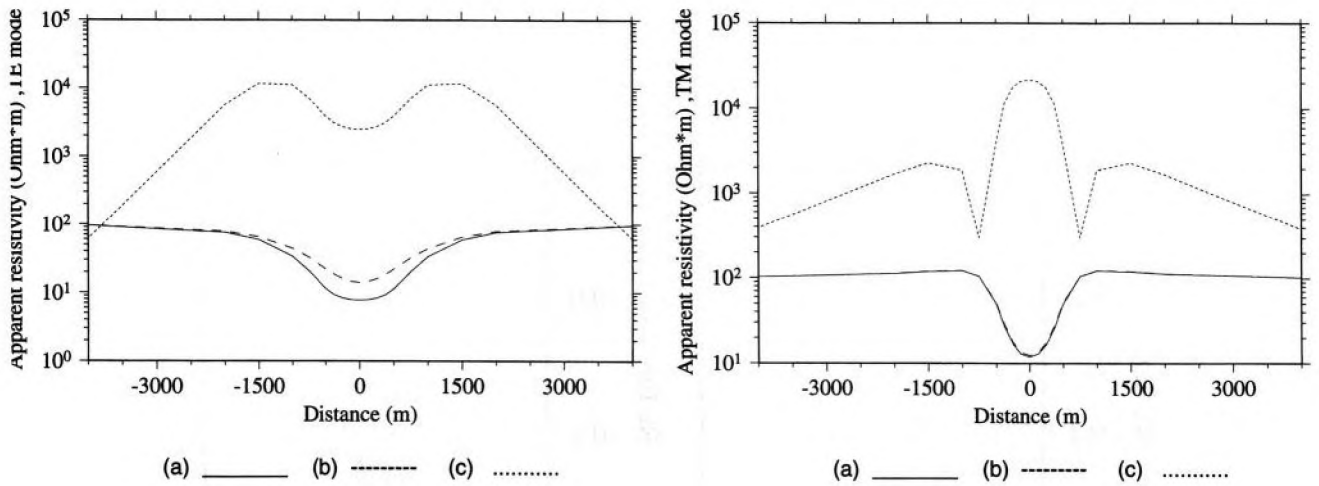

FIG. 9. Numerical comparison of full IE solution (a), QL approximation (b), and Born approximation (c) computed for Model 2 (Figure 7) at the frequency $f = \omega/2\pi = 1$ Hz. Calculations are done for the receivers located along the Y-axis on the surface. Plots present apparent resistivities computed for TM mode (p,) and TE mode (p,).

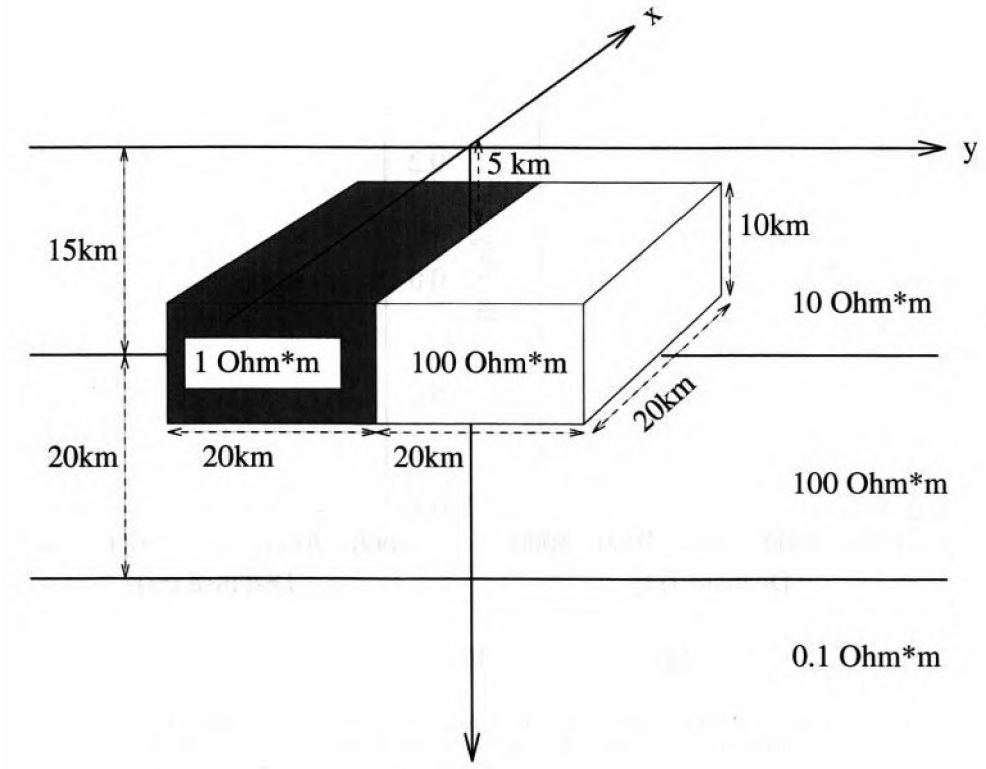

Model 3

FIG. 10.3-D geoelectric model containing two anomalous bodies with different resistivities-1 ohm · m and 100 ohm · m-immersed in a 3-layer earth (Model 3). Model is excited by a vertically propagating plane EM wave.

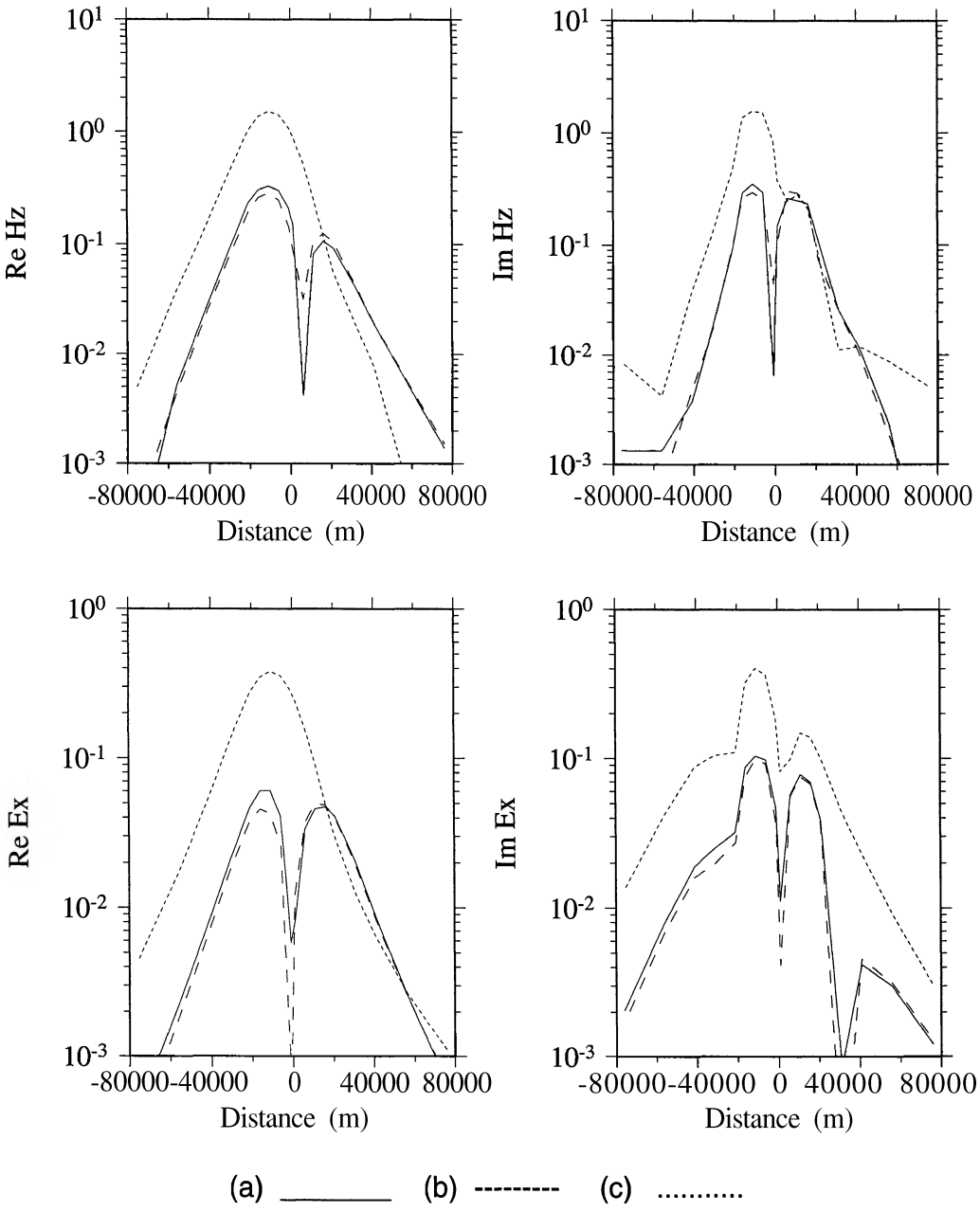

FIG. 11. Numerical comparison of full IE solution (a), QL approximation (b), and Born approximation (c) computed for Model 3 (Figure 10) at the frequency $f = \omega/2\pi = 0.0\ 1$ Hz. Calculations are done for receivers located along the Y-axis on the surface. Plots present real and imaginary components of the electric and magnetic fields.

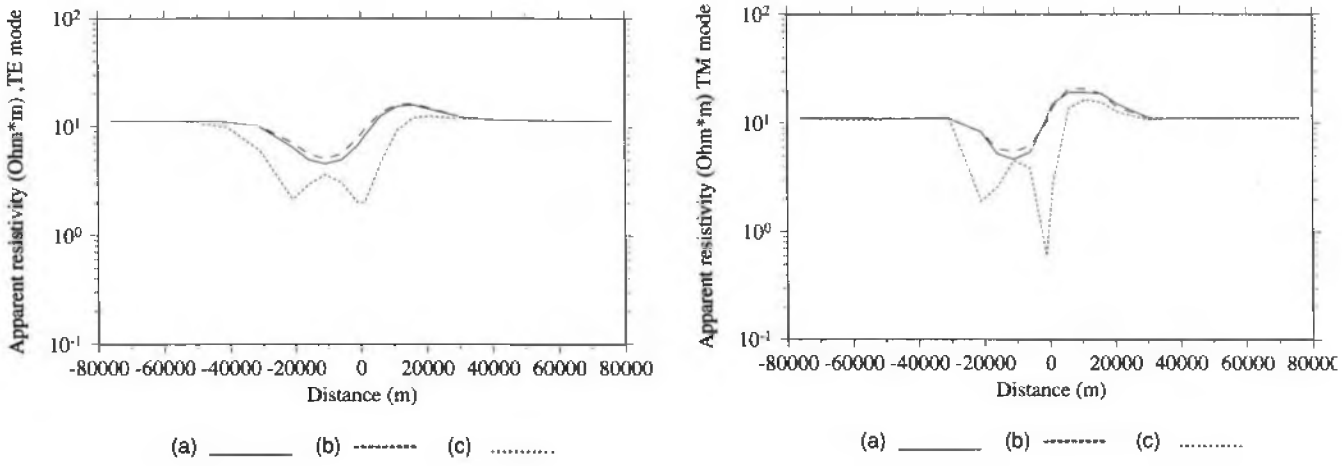

FIG. 12. Numerical comparison of full IE solution (a), QL approximation (b), and Born approximation (c) computed for Model 3 (Figure 10) at the frequency $f = \omega/2\pi = 0.01$ Hz. Calculations are done for receivers located along the Y-axis on the surface. Plots present apparent resistivities computed for TM mode (p,) and TE mode (p,).

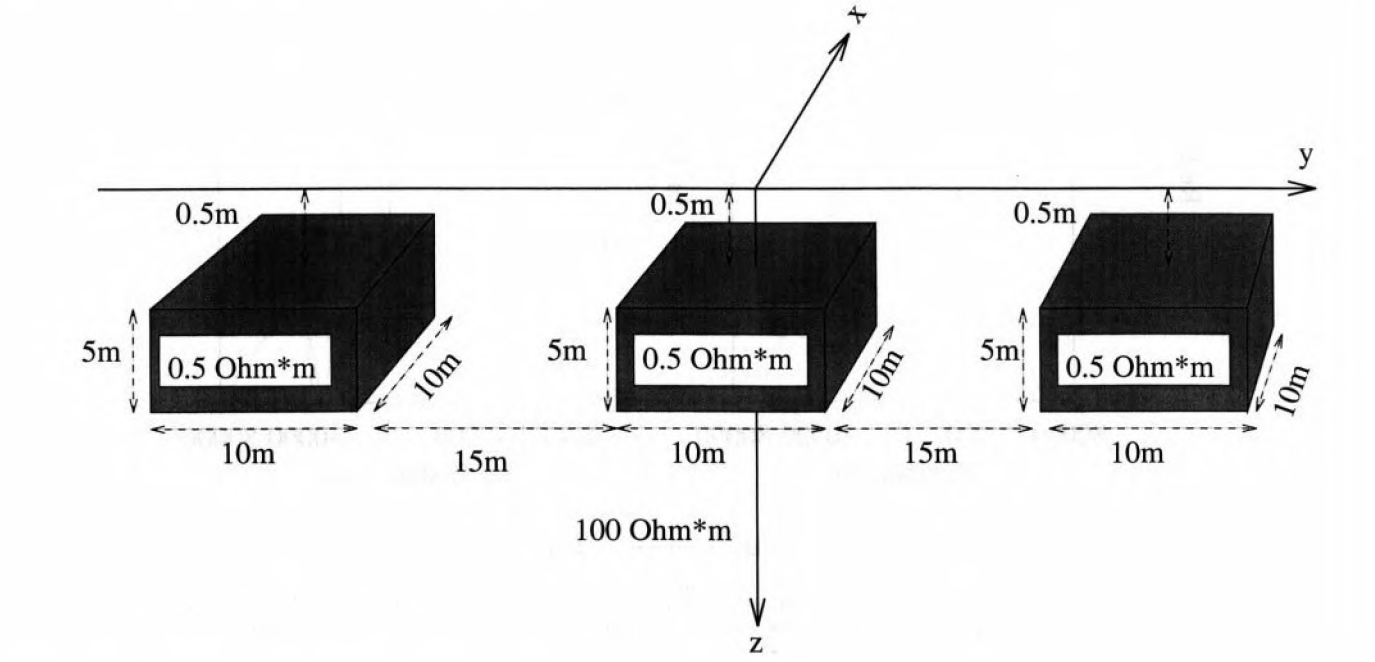

FIG. 13. 3-D geoelectric model containing three conductive bodies in a homogeneous half-space with a plane-wave excitation (Model 4).

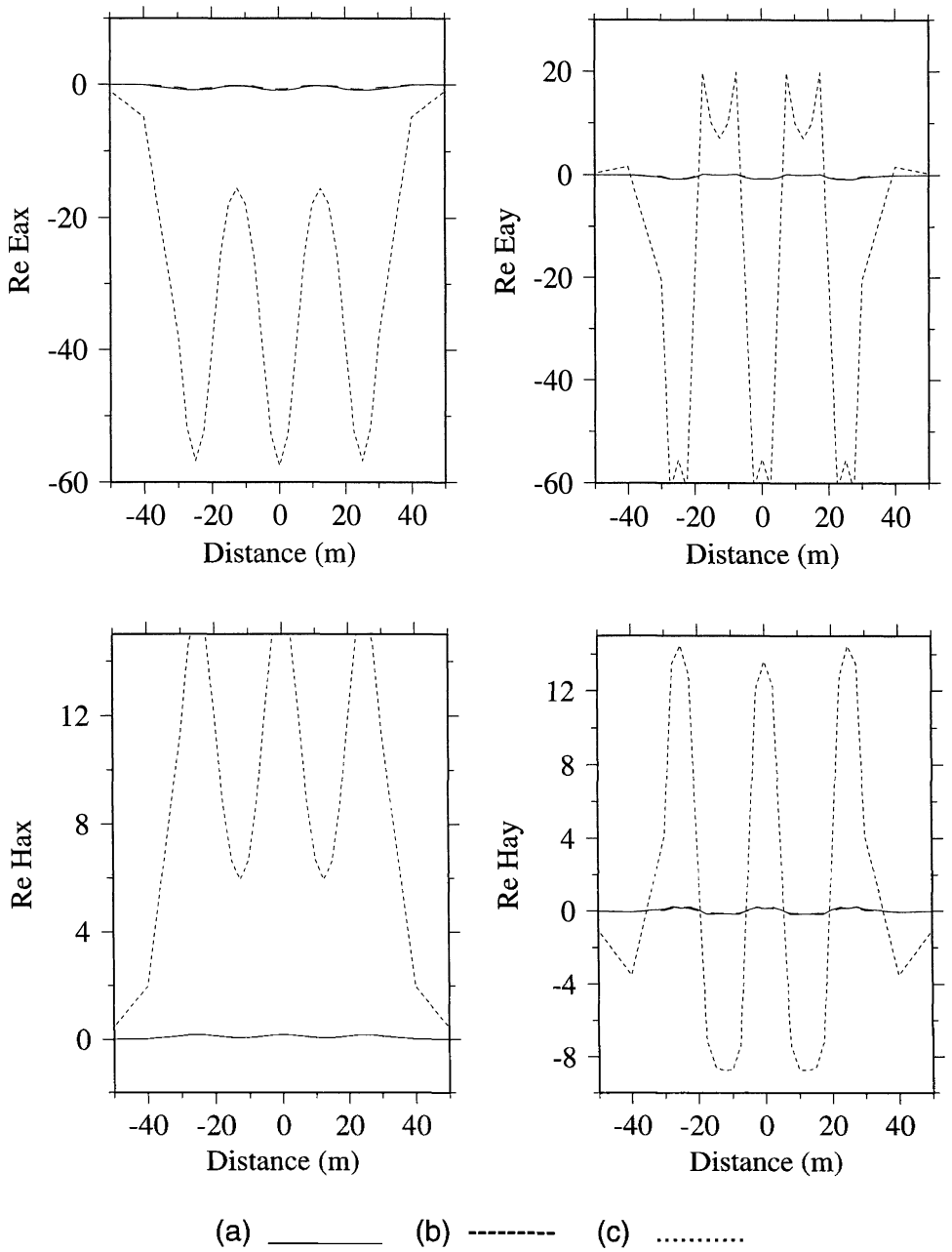

FIG. 14a. Numerical comparison of full IE solution (a), QL approximation (b), and Born approximation (c) computed for Model 4 (Figure 13) at the frequency $f = \omega/2\pi =$ 500 KHz. Calculations are done for receivers located along the Y-axis on the surface. Plots present real and imaginary components of the electric and magnetic fields.

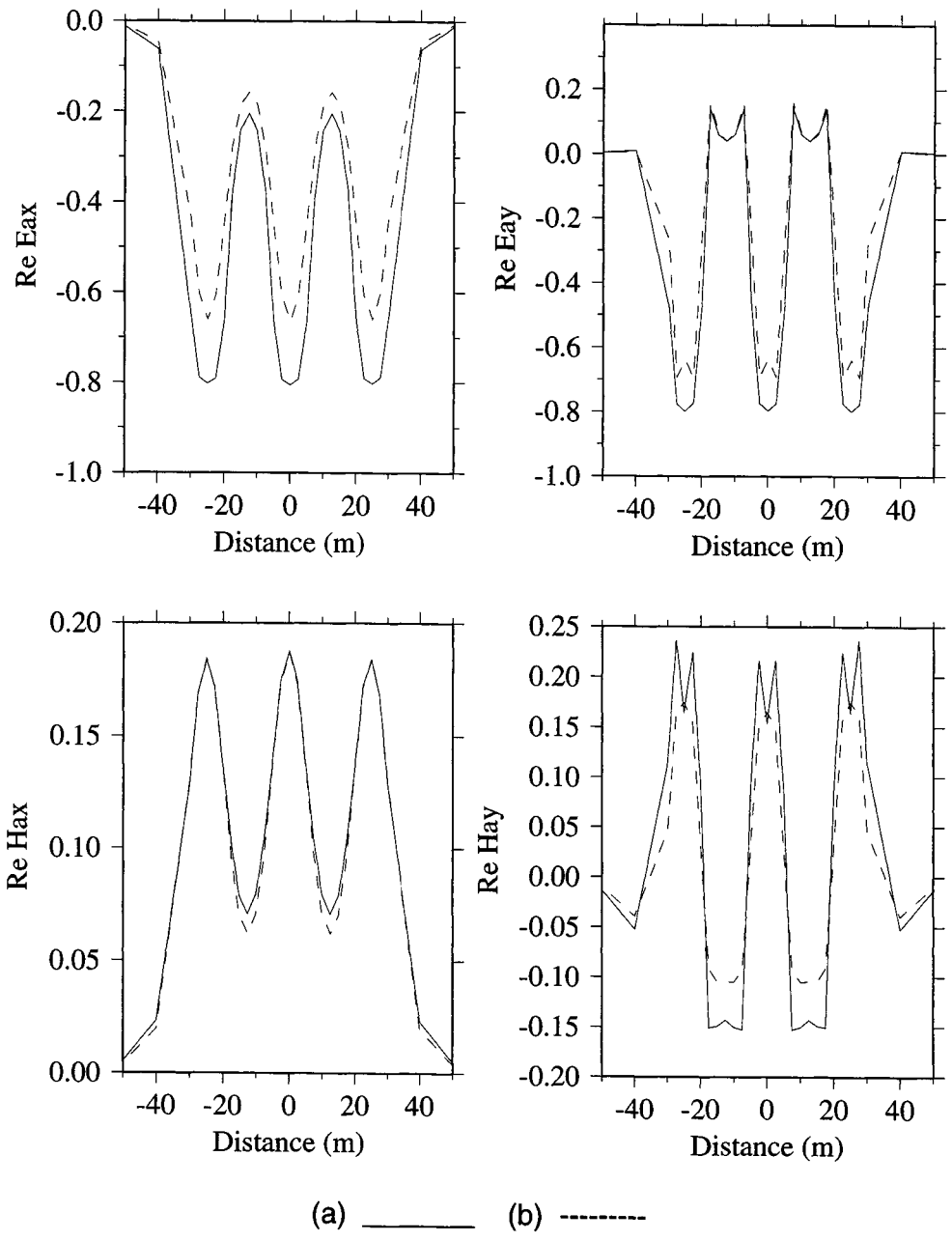

FIG. 14b. Numerical comparison of full IE solution (a) and QL approximation (b) computed for Model 4 (Figure 13) at the frequency $f = \omega/2\pi = 500$ KHz. Calculations are done for receivers located along the Y-axis on the surface. Plots present real and imaginary components of the electric and magnetic fields at a larger vertical scale than in Figure 14a.

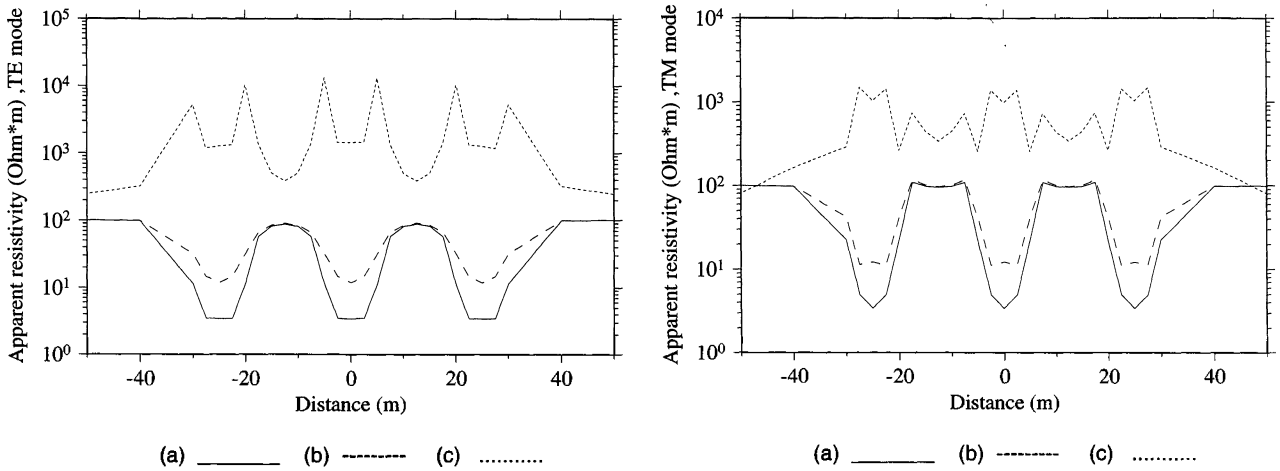

FIG. 15. Numerical comparison of full IE solution (a), QL approximation (b), and Born approximation (c) computed for Model 4 (Figure 13) at the frequency $f = \omega/2\pi = 500$ KHz. Calculations are done for receivers located along the Y-axis on the surface. Plots present apparent resistivities computed for TM mode (p,) and TE mode (ρ_{xy}).

Table 1. Comparison of the CPU time (in seconds) for EM modeling, using different methods (Model 1).

Cell number in anomalous domain	250 cells	400 cells	800 cells
Full integral equation solution	1029.1	2995.0	13127.0
Quasi linear approximation	382.4	530.4	1170.1
Born approximation	237.5	308.5	482.8

Table 2. Comparison of the CPU time (in seconds) for EM modeling, using different methods (Model 2).

Cell number in anomalous domain	250 cells	400 cells	800 cells
Full integral equation solution	1064.6	4785.3	18370.3
Quasi linear approximation	444.9	672.4	1049.5
Born approximation	233.9	352.2	462.0

REFERENCES

Berdichevsky, M. N., and Zhdanov, M. S., 1984, Advanced theory of deep geomagnetic sounding: Elsevier Science Publ. Co., Inc.

Bleistein, N., 1984, Mathematical methods for wave phenomena: Academic Press Inc.

Bleistein, N., and Gray, S. H., 1985, An extension of the Born inversion method to a depth-dependent reference profile: Geophys. Prosp., **33,** 999-1022.

Born, M., 1933, Optic: Springer Publ. Co., Inc.

Born, M., and Wolf, E., 1980, Principles of optics: Pergamon Press, Inc.

Habashy, T. M., Chew, W. C., and Chow, E. Y., 1986, Simultaneous reconstruction of permittivity and conductivity profiles in a radially inhomogeneous slab: Radio Sci., **21,** No. 4, 635-645.

Habashy, T. M., Groom, R. W., and Spies, B. R., 1993, Beyond the Born and Rytov approximations: A nonlinear approach to electromagnetic scattering: J. Geophys. Res., **98,** No. B2, 1759-1775.

Hohmann, G. W., 1975, Three-dimensional induced polarization and electromagnetic modeling: Geophysics, **40,** 309 -324.

Oristaglio, M. L., 1989, An inverse scattering formula that uses all the data: Inverse Problems, **5,** 1097-1105.

Tarantola, A., 1987, Inverse problem theory: Elsevier Science Publ. Co., Inc.

Torres-Verdin, C., and Habashy, T. M., 1994, Rapid 2.5-dimensional forward modeling and inversion via a new scattering approximation, Radio Sci., **29,** No. 4, 1051-1079.

Weidelt, P., 1975, Electromagnetic induction in three-dimensional structures: J. Geophys., **41,** 85-109.

Xiong, Z., 1992, Electromagnetic modeling of three-dimensional structures by the method of system iterations using integral equations: Geophysics, **57,** 1556-1561.

Zhdanov, M. S., 1988, Integral transforms in geophysics: Springer Publ. Co., Inc.

Zhdanov, M. S., and Keller, G. V., 1994, The geoelectrical methods in geophysical exploration: Elsevier Science Publ. Co., Inc.

APPENDIX A

CALCULATION OF THE CONSTANT REFLECTMTY TENSOR

The reflectivity tensor should solve the minimization problem described by equation (35). To develop a solution for this equation, we calculate the first variation of the functional $\varphi(\hat{\lambda})$ as

$$\delta\varphi(\hat{\lambda}, \delta\hat{\lambda}) = -2 \text{ Re } \delta\lambda^*_{\beta\gamma} \sum_{j=1} \Delta E^*_{\alpha\beta\gamma}(\mathbf{r}_j) \times [E^B_\alpha(\mathbf{r}_j) - \lambda_{\mu\nu}\Delta E_{\alpha\mu\nu}(\mathbf{r}_j)]. \quad \text{(A-1)}$$

The minimum of equation (35) is reached when $\delta\varphi(\hat{\lambda}, \delta\hat{\lambda}) \equiv 0$ for any $\delta\hat{\lambda}$. Therefore

$$\lambda_{\mu\nu} \sum_{j=1}^{J} \Delta E^*_{\alpha\beta\gamma}(\mathbf{r}_j)\Delta E_{\alpha\mu\nu}(\mathbf{r}_j) = \sum_{j=1}^{J} \Delta E^*_{\alpha\beta\gamma}(\mathbf{r}_j) E^B_\alpha(\mathbf{r}_j), \quad \text{(A-2)}$$

where $\beta, \gamma = x, y, z$.

Thus, we have:

$$[\lambda_{\mu\nu}] = \left[\sum_{j=1}^{J} \Delta E^*_{\alpha\beta\gamma}(\mathbf{r}_j)\Delta E_{\alpha\mu\nu}(\mathbf{r}_j) \right]^{-1} \times \left[\sum_{j=1}^{J} \Delta E^*_{\alpha\beta\gamma}(\mathbf{r}_j)\ E^B_\alpha(\mathbf{r}_j) \right]. \quad \text{(A-3)}$$

For example in the simplest case when $\hat{\lambda}$ is a scalar tensor,

$$\lambda_{\beta\gamma} = \lambda\delta_{\beta\gamma}, \quad \text{(A-4)}$$

we can find immediately from equation (A-l) that

$$\delta\varphi(\hat{\lambda}, \delta\hat{\lambda}) = -2 \text{ Re } \delta\lambda^* \sum_{j=1} \Delta E^*_{\alpha\beta\beta}(\mathbf{r}_j) \times [E^B_\alpha(\mathbf{r}_j) - \lambda\Delta E_{\alpha\mu\mu}(\mathbf{r}_j)] \quad \text{(A-5)}$$

and

$$\lambda = \frac{\sum_{j=1}^{J} \Delta E^*_{\alpha\beta\beta}(\mathbf{r}_j) E^B_\alpha(\mathbf{r}_j)}{\sum_{j=1}^{J} \Delta E^*_{\alpha\beta\beta}(\mathbf{r}_j)\Delta E_{\alpha\mu\mu}(\mathbf{r}_j)}. \quad \text{(A-6)}$$

When $\hat{\lambda}$ is a diagonal tensor

$$\lambda_{\beta\gamma} = \begin{cases} \lambda_\beta, & \beta = \gamma \\ 0, & \beta \neq \gamma \end{cases} \quad \text{(A-7)}$$

we can find immediately from equation (A-5) that

$$\delta\varphi(\hat{\lambda}, \delta\hat{\lambda}) = -2 \text{ Re } \delta\lambda^*_\beta \sum_{j=1} \Delta E^*_{\alpha\beta}(\mathbf{r}_j) \times [E^B_\alpha(\mathbf{r}_j) - \lambda_\mu \Delta E_{\alpha\mu}(\mathbf{r}_j)], \quad \text{(A-8)}$$

where

$$\Delta E^*_{\alpha\beta}(\mathbf{r}_j) = \Delta E^*_{\alpha\overline{\beta}\beta}(\mathbf{r}_j).$$

The line above β means no summation over β.

Equation (A-2) then takes the form

$$\lambda_\mu \sum_{j=1}^{J} \Delta E^*_{\alpha\beta}(\mathbf{r}_j)\Delta E_{\alpha\mu}(\mathbf{r}_j) = \sum_{j=1}^{J} \Delta E^*_{\alpha\beta}(\mathbf{r}_j) E^B_\alpha(\mathbf{r}_j). \quad \text{(A-9)}$$

Solving equation (A-9) we find

$$[\lambda_\mu] = \left[\sum_{j=1}^{J} \Delta E^*_{\alpha\beta}(\mathbf{r}_j)\Delta E_{\alpha\mu}(\mathbf{r}_j) \right]^{-1} \times \left[\sum_{j=1}^{J} \Delta E^*_{\alpha\beta}(\mathbf{r}_j) E^B_\alpha(\mathbf{r}_j) \right]. \quad \text{(A-10)}$$

In the general case we should solve equation (A-3) to find $\hat{\lambda}$.

APPENDIX B

CALCULATION OF THE VARIABLE REFLECTIVITY TENSOR

We rewrite equation (43) for the points inside domain D_k, taking into account equation (42):

$$E^s_\alpha(\mathbf{r}_j) = \lambda^k_{\beta\gamma}\delta_{k\ell}\delta_{\alpha\beta}E^n_\gamma(\mathbf{r}_j) = \sum_{k=1,K} (\delta_{\beta\gamma} + \lambda^k_{\beta\gamma}) \iiint_D G^n_{\alpha\beta}(\mathbf{r}_j|\mathbf{r})\widetilde{\Delta\sigma}(\mathbf{r}) E^n_\gamma(\mathbf{r})\, dv \quad \text{(B-1)}$$

$$\mathbf{r}_j \in D_\ell.$$

Therefore we have

$$\sum_{k=1,K} \lambda^k_{\beta\gamma} \left[\delta_{k\ell}\delta_{\alpha\beta}E^n_\gamma(\mathbf{r}_j) - \iiint_{D_k} G^n_{\alpha\beta}(\mathbf{r}_j|\mathbf{r})\widetilde{\Delta\sigma}(\mathbf{r}) E^n_\gamma(\mathbf{r})\, dv \right] = \mathbf{E}^B_\alpha(\mathbf{r})\, dv, \quad \text{(B-2)}$$

where $\mathbf{r}_j \in D_\ell$.

The last equation provides the basis for determining $\hat{\lambda}^k$. This equation should hold for any internal point within the domain D. In reality, of course it holds only approximately. Therefore, we can use the least-squares method to determine the $\hat{\lambda}^k$ that fits equation (B-2) to the highest accuracy:

$$\varphi(\hat{\lambda}) = \sum_{j=1}^{J} [E^B_\alpha(\mathbf{r}_j) - \lambda^k_{\beta\gamma}\Delta E_{\alpha\beta\gamma k}(\mathbf{r}_j)]^* \times [E^B_\alpha(\mathbf{r}_j) - \lambda^m_{\mu\nu}\Delta E_{\alpha\mu\nu m}(\mathbf{r}_j)] = \min \quad \text{(B-3)}$$

Here

$$k, m = 1, 2, \ldots K$$

$$\alpha, \beta, \gamma, \mu, \nu = x, y, z$$

and

$$\Delta E_{\alpha\beta\gamma k}(\mathbf{r}_j) = \delta_{\alpha\beta}\delta_{k\ell}E^n_\gamma(\mathbf{r}_j) - \int\int\int_{D_k} G_{k\,\alpha\beta}{}^n(\mathbf{r}_j|\mathbf{r})\tilde{\Delta}\sigma(\mathbf{r})E^n_\gamma(\mathbf{r})\,dv, \quad \text{(B-4)}$$

where $\mathbf{r}_j \in D_\ell$.

The symbol * denotes complex conjugation.

We calculate the first variation of the functional $\varphi(\hat{\lambda})$ as

$$\delta\varphi(\hat{\lambda}, \delta\hat{\lambda}) = -2\,\mathrm{Re}\,\delta\lambda^k_{\beta\gamma}\sum_{j=1}^{J}\Delta E^*_{\alpha\beta\gamma k}(\mathbf{r}_j) \times [E^B_\alpha(\mathbf{r}_j) - \lambda^m_{\mu\nu}\Delta E_{\alpha\mu\nu m}(\mathbf{r}_j)], \quad \text{(B-5)}$$

where the minimum of (B-3) is reached when $\delta\varphi(\hat{\lambda}, \delta\hat{\lambda}) \equiv 0$ for any $\delta\hat{\lambda}$. Therefore

$$\lambda^m_{\mu\nu}\sum_{j=1}^{J}\Delta E^*_{\alpha\beta\gamma k}(\mathbf{r}_j)\Delta E_{\alpha\mu\nu m}(\mathbf{r}_j) = \sum_{j=1}^{J}\Delta E^*_{\alpha\beta\gamma k}(\mathbf{r}_j)E^B_\alpha(\mathbf{r}_j), \quad \text{(B-6)}$$

where $k, m = 1, 2, \ldots K$; $\alpha, \beta, \gamma, \mu, \nu = x, y, z$.

Thus, we have

$$[\lambda^m_{\mu\nu}] = \left[\sum_{j=1}^{J}\Delta E^*_{\alpha\beta\gamma k}(\mathbf{r}_j)\Delta E_{\alpha\mu\nu m}(\mathbf{r}_j)\right]^{-1} \times \left[\sum_{j=1}^{J}\Delta E^*_{\alpha\beta\gamma k}(\mathbf{r}_j)E^B_\alpha(\mathbf{r}_j)\right]. \quad \text{(B-7)}$$

The last expression is the solution for the problem of the reflectivity tensor $\hat{\lambda}^m$ determination for every subdomain D_m of the structure D with anomalous conductivity.